

Numerical Simulation Of Flow Characteristics For Three Wind Turbines With Inverted-Triangle Distribution Under Yaw Condition

*Haocheng SUN¹⁾ and Peng HUANG²⁾

^{1), 2)} State Key Laboratory of Disaster Reduction in Civil Engineering, Tongji University,
Shanghai 200092, China
²⁾ huangtju@tongji.edu.cn

ABSTRACT

Wind flowing through wind turbines results in the wind velocity decreasing and turbulence intensity rising. The wake of wind turbines arranged in wind farm interferes with each other, which is a significant and complex phenomenon for output power. In this study, the wake interference of wind turbines in different rows is analyzed by CFD simulation. Three wind turbines with inverted-triangle distribution in wind farm were chose as an analytical unit, considering the influence of different yaw angles to the flow field. The Actuator Line Model (ALM) combined with CFD technique is applied to simulate rotational blades, and this solver is verified with the Large Eddy Simulation (LES) results. The results reveal the flow characteristics, wake behaviors and facility performance of three wind turbines with inverted-triangular distribution in the case of maintaining the longitudinal and horizontal spacing in wind farm, and provide a reference value to spatial layout of the complete wind farm.

1. INTRODUCTION

Wind energy is a well-developed renewable energy. In recent year, global wind power generation increased thirty per cent per year approximately^[1]. When studying in generated power and load, a distinct division is generally made into the near and far wake region according to different wake characteristics^[2]. The near wake region is taken as the area behind the rotor approximately one rotor-diameter distance downstream, and the wake characteristics is mainly affected by geometry. However, the effect of large Reynolds number and geometry is weakened in the far wake region, and the reduction of wind velocity follows the Gaussian distribution^[3]. There exists many serve influences to the wind turbines downstream in wind farm due to wind velocity reduction and large Reynolds number caused by wake effect, containing attenuation of power generation and increasing the fatigue load on blades^[4, 5].

Computational fluid dynamics method (CFD) has been a common method to acquire aerodynamic performances of wind turbines, and LES method with simplified boundary conditions is generally used for simulating the turbulence in the flow field^[7]. However, LES method requires a large amount of computation. Blade Element

¹⁾ graduate student.

²⁾ professor, Corresponding Author

Momentum theory (BEM), which is generally considered as an effective method, cannot solve wake characteristics, and the results of the vortex method to small scaled eddy is inaccurate^[6]. The Actuator Method, which could simulate blades under the running state of wind turbine, mainly contains Actuator Disk Model (ADM), Actuator Line Model (ALM) and Actuator Surface Model (ASM). The main difference among three types lies in the treatment to aerodynamic force on blades. ADM distributes blade aerodynamic force uniformly along the annular direction, while ALM distributes blade aerodynamic force along the radial direction, and ASM takes it as the equivalent surface force^[3]. The vortex shedding of its wake is continuous using ADM. Nevertheless, the actual wind turbine wake structure is very complex, and the assumption that the aerodynamic force is uniformly distributed along the annular direction is obviously unreasonable. Precision of ASM is the best among the three, but its number of calculations is large and the costs are expensive. As for ALM, it could calculate more precise than ADM. Meanwhile, the process of modelling is much simpler than ASM, and it meet engineering requirement better.

Yaw could change flow filed considerably in wind farm. Active yawing to upstream wind turbines deviates wakes from downstream blades, which could weaken wake effect to a certain extent. Jiménez et al. (2010) studied the track deviation of a single wind turbine at different yaw angles and thrust coefficients using large eddy simulation^[8]. KROGSTAD et al. (2013) researched the wake behavior of a single wind turbine based on wind tunnel tests comparing BEM method and CFD method^[9]. Krogstad and PIERELLA et al. (2015) studied the flow characteristics of two wind turbines under different spacing arrangements^[10, 11]. Fleming et al. (2015) compared the performance of two wind turbines under the conditions of different yaw angles, tilt angles^[12]. Draper et al. (2018) studied the active yawing control of three wind turbines in series by analyzing their flow characteristics, wake behavior and facility performance^[13]. In the actual wind farm, the wind turbines wake caused by yaw is superimposed, which makes the study on spatial layout more complicated.

In this paper, three wind turbines with inverted-triangle distribution in wind farm were chose as an analytical unit, considering the influence of different yaw angles to the flow field, which is illustrated in Fig. 1. The Actuator Line Model (ALM) combined with CFD technique is applied to simulate rotational blades. This paper seeks to research the wake interference of wind turbines in different rows, and contribute to optimize the spatial layout of the complete wind farm.

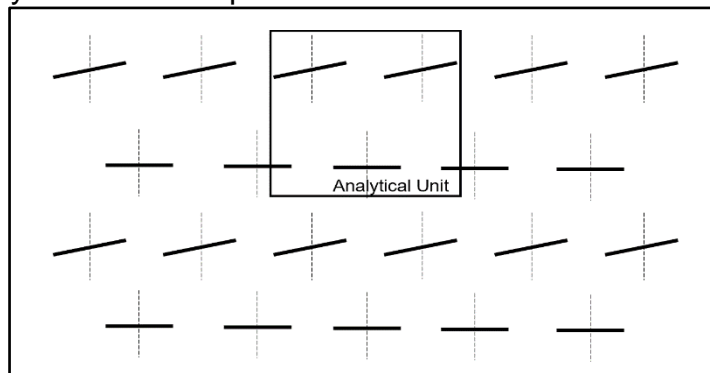


Fig. 1 Analytical Unit in Wind Farm

2. ACTUATOR LINE MODEL

Actuator line method is an application combining blades element momentum theory with CFD technique. The basic idea of this method is replacing blades in the running states with the lines, which volume force acts on, along the radial direction of blades. Adding a volume force source term to average Navier-Stokes equations represents the force of blades acting on the fluid^[14]. This method could avoid solving boundary layer of blades with constantly moving grid, and save computation largely, meanwhile its accuracy is also ensured.

2.1 Governing Equations

The governing equations used for numerical simulation are incompressible RANS equations, which is shown in Eq. (1).

$$\frac{\partial}{\partial t} \left(r u_i \right) + \frac{\partial}{\partial x_i} \left(r u_i u_j \right) = - \frac{\partial}{\partial x_i} \left[m \frac{\partial u_i}{\partial x_j} - r \overline{u_i u_j} \right] + S_i \quad (1)$$

where m is the viscosity coefficient of fluid, S_i is the body force source, and $-r \overline{u_i u_j}$ denotes the Reynolds stress. In order to obtain the closed solution, Boussinesq hypothesis is proposed to explain Reynolds stress, which is expressed in Eq. (2).

$$-r \overline{u_i u_j} = m_t \left(\frac{\partial u_i}{\partial x_j} + \frac{\partial u_j}{\partial x_i} \right) - \frac{2}{3} \left(rk + m_t \frac{\partial u_i}{\partial x_i} \right) d_{ij} \quad (2)$$

where μ_t denotes the turbulent viscosity, u_i is the time-averaged velocity, and k represents the turbulence kinetic energy.

Compared with the standard $k-\varepsilon$ model, in order to improve the simulation accuracy of the abrupt flow and eddy region, the RNG $k-\varepsilon$ model is adopted much reasonably, which is shown in Eq. (3), (4).

$$\frac{\partial}{\partial t} \left(rk \right) + \frac{\partial}{\partial x_i} \left(r k u_i \right) = \frac{\partial}{\partial x_j} \left(\alpha_k m \frac{\partial k}{\partial x_j} \right) + G_k + G_b - re - Y_M + S_k \quad (3)$$

$$\frac{\partial}{\partial t} \left(re \right) + \frac{\partial}{\partial x_i} \left(r e u_i \right) = \frac{\partial}{\partial x_j} \left(\alpha_e m \frac{\partial e}{\partial x_j} \right) + C_{1e} \frac{e}{k} \left(G_k + C_{3e} G_b \right) - C_{2e} r \frac{e^2}{k} - R_e + S_e \quad (4)$$

where α_k and α_e are the inverse effective Prandtl numbers of k and ε , respectively.

2.2 Volume Force Source Term

The solution of volume force source term is based on the blade element momentum theory (BEM), that is, the attack angle of the airfoil in the flow field is extracted in each time step, and the force of the airfoil segment can be obtained from

the aerodynamic performance. A two-dimensional airfoil cross-section at radius r is shown as Fig. 2, and the relative velocity to the rotating blade is expressed in Eq. (5).

$$V_r = \left[V_z^2 + (V_q - Wr)^2 \right]^{\frac{1}{2}} \quad (5)$$

where Ω is the angle velocity of the rotating blade, and r denotes the length of radial direction to the airfoil local position.

The attack angle is defined as Eq. (6).

$$\alpha = j - g \quad (6)$$

where φ denotes the angle between the relative velocity and horizontal axis, and γ denotes the local pitch angle.

The volume force of local positions in blade element could be illustrated in Eq. (7).

$$f = \frac{dF_i}{dr} = \frac{1}{2} r V_r^2 c (C_L e_L + C_D e_D) \quad (7)$$

where C_L and C_D are the lift and drag coefficients, respectively, e_L and e_D denote the unit direction vectors of the lift and drug, respectively, and c is the chord length.

Since the volume force at each local position is discrete, the distribution of volume force on the airfoil is rough. Avoiding non-convergence of these equations in the period of calculating, it should be smoothed, and the convolution between the regularized kernel function and volume force is generally adopted to smooth it, which is shown in Eq. (8).

$$S_{e,i}(x, y, z, t) = f * h_i = \sum_{j=1}^N f(x_j, y_j, z_j, t) \frac{1}{\pi r_i^3} \exp \left[-\left(\frac{r_i}{l} \right)^2 \right] \quad (8)$$

where $f(x_j, y_j, z_j, t)$ denotes local volume force before smoothing, r_i is defined as the relative distance between the local position and base point, and l denotes smooth coefficient, generally valued $2Dx$. Dx is the grid size at the blade.

Some physical quantities, such as velocity and pressure, could be solved in the flow field by adding volume force source term calculated by Eq. (8) into the governing equations.

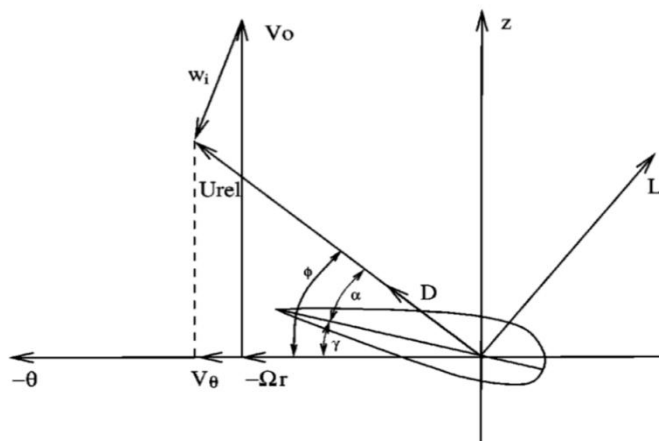


Fig. 2^[14] Two-dimensional Airfoil Cross-section

3. MODEL VERIFICATION

NREL phase VI wind turbine is chosen as the research object, for which there exists abundant data, and the main parameters are shown in the Table 1. JangOh et al. (2013) [15] builds the full-scale grid model using the sliding mesh method of FLUENT. The facility performance and flow characteristics of a single wind turbine is simulated by S-A Dynamic Sub-grid Scale model. And the validity of the ALM is verified, compared with the results of LES^[16].

Table 1 Main Parameters of NREL Phase VI Wind Turbine

Blade Number	2
Rotor Diameter, m	10.058
Rotor Speed, rad/s	1.2
Rated Power, kW	19.8
Airfoil	S809
Pitch Angle	3

3.1 The Numerical setting

the length along the flow direction is $17D$. The width and height are the same as the size of the wind tunnel: $24.4m \times 36.6m$, and the distance between the entrance and the model is $2D$. the mesh of which the distribution is the densest is situated at the near region, of which size is $7D \times 1.5D \times 1.5D$. the number of the grid substituting rotational blades is about thirty, and the grid of the other region turn sparse proportionally along the direction of boundary.

The inlet condition is set as uniform inflow, and the axial velocity is $7m/s$. According to the NREL wind tunnel test and LES simulation conducted by JangOh, the turbulence intensity at the inlet is 0.2% , and the upper boundary is the same as the inlet. Besides, the outlet condition is set as free outflow, and the side boundary is set as symmetric boundary while the lower boundary as no slip wall boundary.

3.2 The Model Solver

The numerical model is solved by FLUENT commercial software, and the UDF is coded for adding volume force source term to CFD control equations, and changing the position of every rotated blade element according to the tip speed ratio in each cycle. the program flow chart is shown as Fig. 3.

Table 2 The Comparison Between The ALM, LES and Experiment

	Power, KW	Error, %	Thrust, N	Error, %
Experiment	6.048	0	1224	0
LES	5.826	3.67	1177	3.83
ALM	6.621	9.47	1251	2.2

3.3 The Model Comparison

As shown in table 2, the above example used to verify the ALM is compared with the results of full-scale LES simulation. The power value calculated by ALM is 9.47% larger than that of wind tunnel test, and the error of thrust between these reaches 2.2%. The causes of the error are very complicated. The effect of the tower and the engine room on the flow field is neglected, on the other hand, the blade tip loss, blade root loss and delayed stall are not corrected, which also influence the calculating precision. the error basically meets the engineering requirements, especially for the large-scale flow field simulation such as the whole wind farm. Compared with the results of LES full-scale simulation, the power error of ALM is relatively larger, and the thrust calculated by ALM is slightly better than that of LES. ALM has some significant advantages such as less computation and simpler grid division, etc. The precision could be better than that of the full-scale model by constantly modifying the model.

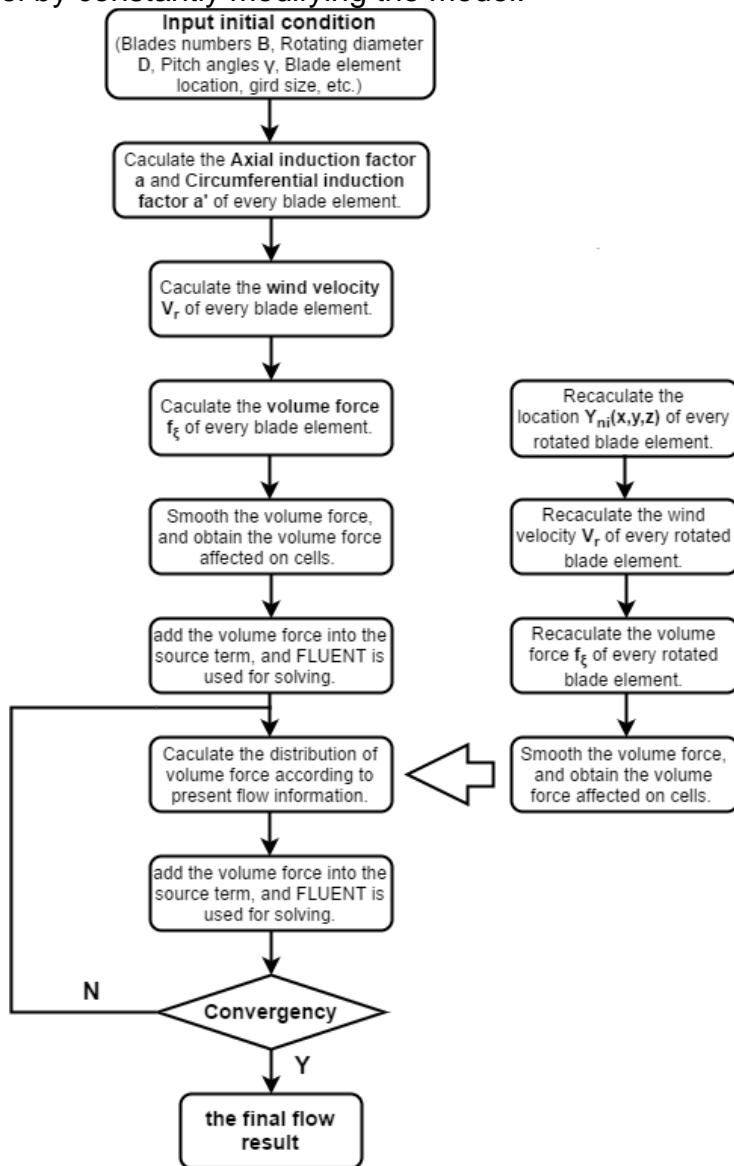


Fig. 3 the UDF Flow Chart

4. THREE WIND TURBINES WITH INVERTED-TRIANGLE DISTRIBUTION

three wind turbines with inverted-triangle distribution are selected as the research objects, of which basic structure are shown in Fig. 4. Maintaining the space of two wind turbine in the first row H as $3D$ and row space L as $5D$. The wake interference effect of downstream wind turbine is observed by altering the stagger distance between the first wind turbine in the first row and downstream one I ^[17]. I increases successively with $D/3$ as a basial unit, and are 0 , $D/3$, $2D/3$, D , $4D/3$, $3D/2$, respectively in the analytical cases. The location of the downstream wind turbine is from completely in the wake area of the first wind turbine in the first row to the middle of the two wind turbines in the first row.

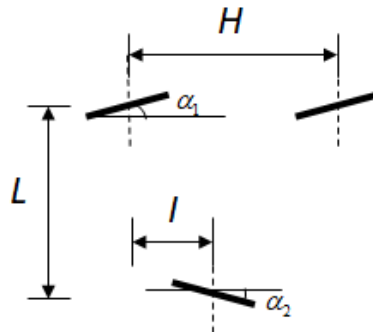


Fig. 4 Three Wind Turbines with Inverted-triangle Distribution

The yaw of the front-row wind turbines has a significant effect on the flow distribution of the wind farm and the performance of the back-row wind turbine. The correlation between the yaw angle and the stagger distance between rows is not taken into account for the time being, and the optimum stagger distance without yaw is maintained. The influence of different yaw angles of front-row wind turbines to the output power of downstream wind turbines is studied, and the yaw angle α_1 is set as 5° , 10° , 15° , 20° , respectively.

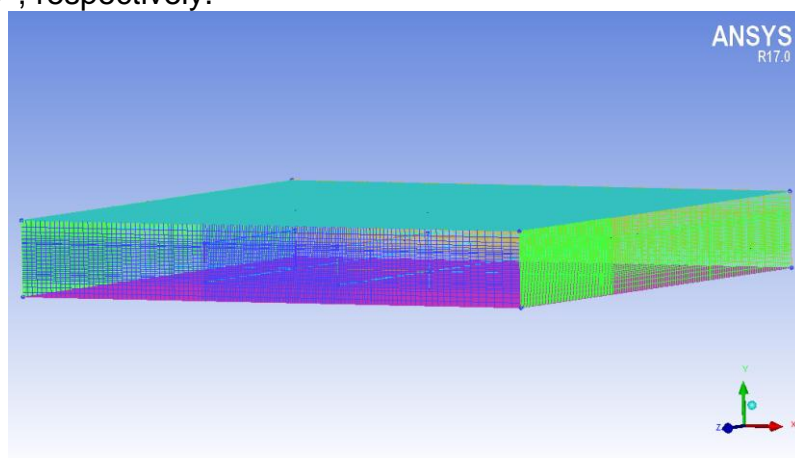


Fig. 5 Computational Domain

To be available for the future research, the computational domain is according to the TJ-3 Boundary Layer Wind Tunnel of Tongji University with $14m \times 15m \times 2m$, which is shown in Fig. 5. The inlet and the upper boundary condition are set as uniform inflow, and the wind speed is $8m/s$. The turbulence intensity at the inlet is 0.2%. Besides, the outlet boundary condition is set as free outflow, and the side boundary is set as symmetric boundary while the lower boundary as no slip wall boundary.

4.1 Determination of The Optimum Stagger Distance without Yaw

Maintaining the fixed space between the different rows and ranks in the wind farm, ALM is adopted to obtain the wake behaviors and facility performance. The profile wind velocity and the output power are shown in Fig. 6 and Fig. 7 respectively.

It can be seen from the wind speed profile at different positions of the rear wind turbine that the wind speed distribution before the downstream one is almost the same under the condition of uniform inflow and without yawing. There is an obvious decrease in wind velocity of incoming flow, which means some of wind energy is transformed into electricity. Velocity distribution of a single wind turbine illustrates that central velocity is relatively high and side velocity is low, which represents the velocity loss near the end of the blade is the most serious, and the velocity at the center of the wind turbine rise slightly. The reason may be that the influence of tower and engine room on the flow field behind the wind turbine is ignored.

For three wind turbines with inverted-triangle distribution, the rear wind turbine is gradually situated from the wake zone of the first one in the front row to the wake interference zone of the two wind turbines as the stagger distance between the first wind turbine in the first row and downstream one increasing. As a result of the wakes expansion, the downstream one is almost located in the wakes interference area of these two in the upstream. Under the premise of no yawing, when the stagger distance is from 0 to $2D/3$, the downstream wind turbine is mainly situated in the wakes area of the first one in the upstream and less affected by the second one. And its output power is relatively low while the growth rate of the power is slow as the stagger distance changing. Therefore, the downstream wind turbine is significantly influenced by the wakes, and its velocity loss is serious. Besides, the asymmetry of the velocity profile is not evident. Meanwhile, the wind pressure acting on the blade structure of the downstream one is relatively large, and the blades is subject to larger volume force of the incoming flow, which inclines to fatigue the structure and reduce its durability. When the stagger distance is from $2D/3$ to $3D/2$, the downstream wind turbine is gradually away from wakes area of the first one in the upstream, and could be viewed as in the corporate wakes area produced by the two upstream wind turbines.

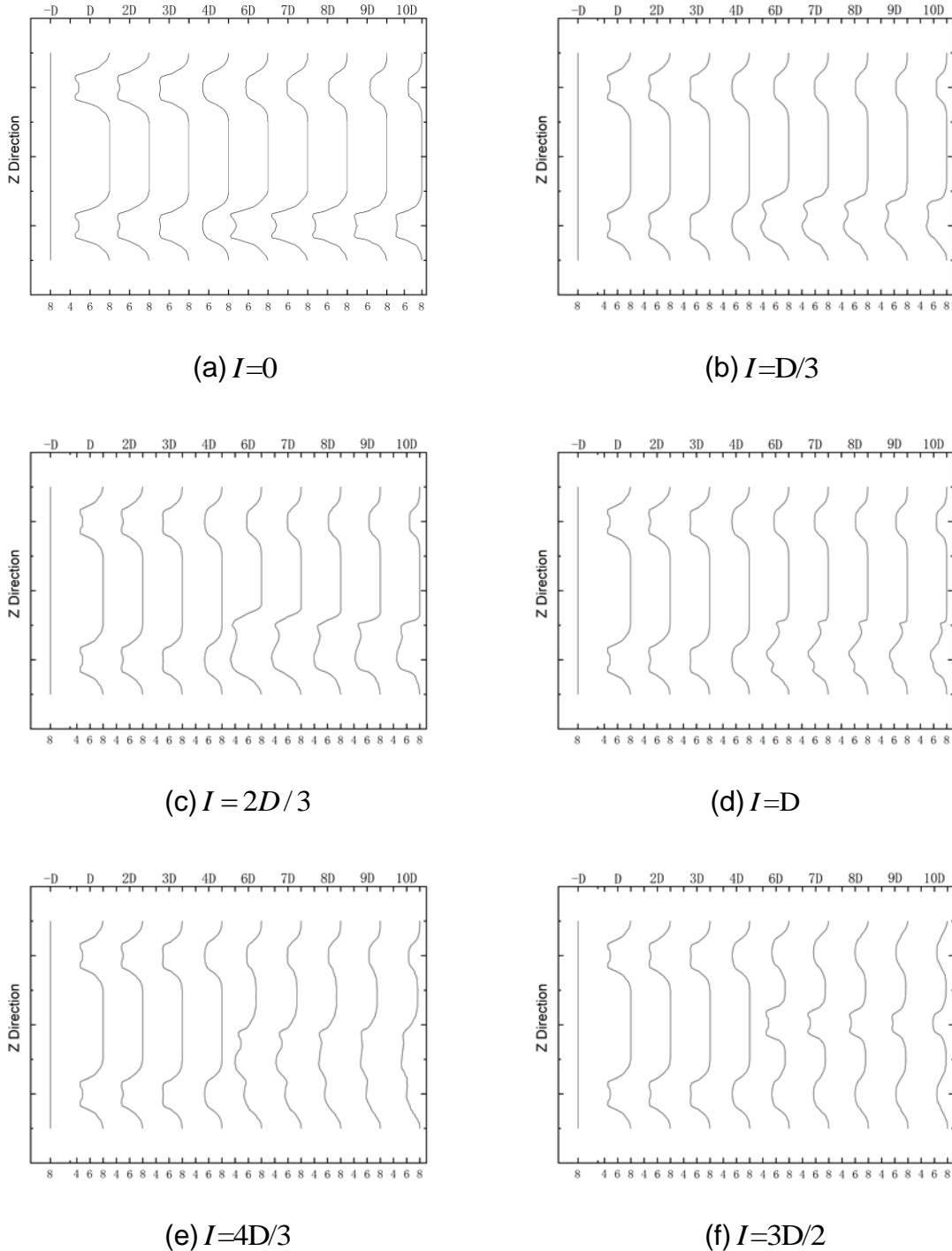


Fig. 6 The Profile Wind Velocity in Different Stagger Distances

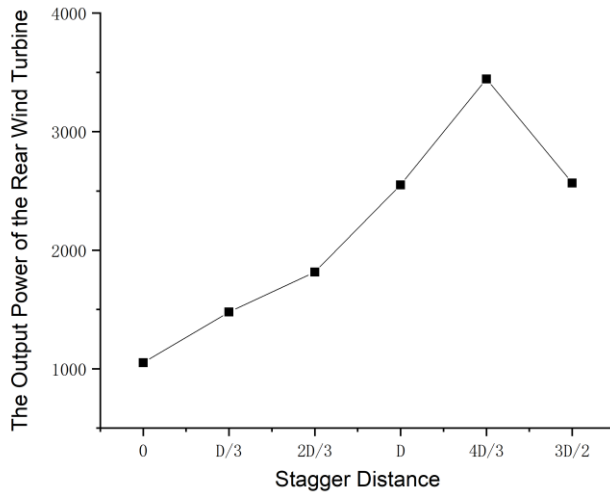


Fig. 7 The Output Power of the Rear Wind Turbine

As increase of stagger distance, the output power of the rear wind turbine increases firstly and reaches to the maximum, and then decreases. Obviously, the optimum stagger distance is $4D/3$. Also, The increase of the output power of the rear wind turbine is the largest, which is 40.6%, when the first $D/3$ is changed. When the stagger distance is from $2D/3$ to $3D/2$, the growing rate of the output power increases to 40.4% dramatically, since the downstream wind turbine leave away from the wakes caused by the first one in the first row nearly.

4.2 Yaw Condition Analysis

When yawing happens in the two front wind turbines of three wind turbines with inverted-triangle distribution, there is an obvious change in wake characteristics, and flow field turns more complicated. In the case of the optimum stagger distance, the speed profile in yaw and the output power are shown in Fig. 8 and Fig. 9 respectively.

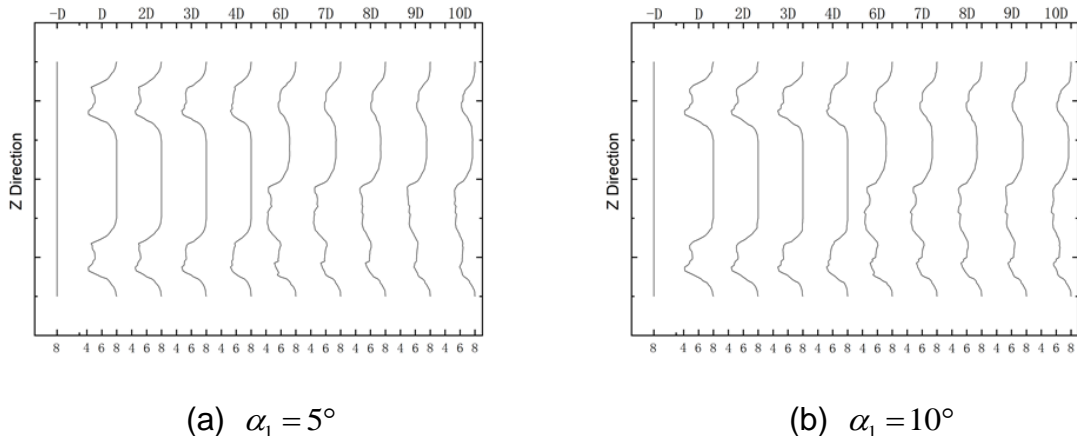


Fig. 8 The Speed Profile in Yaw

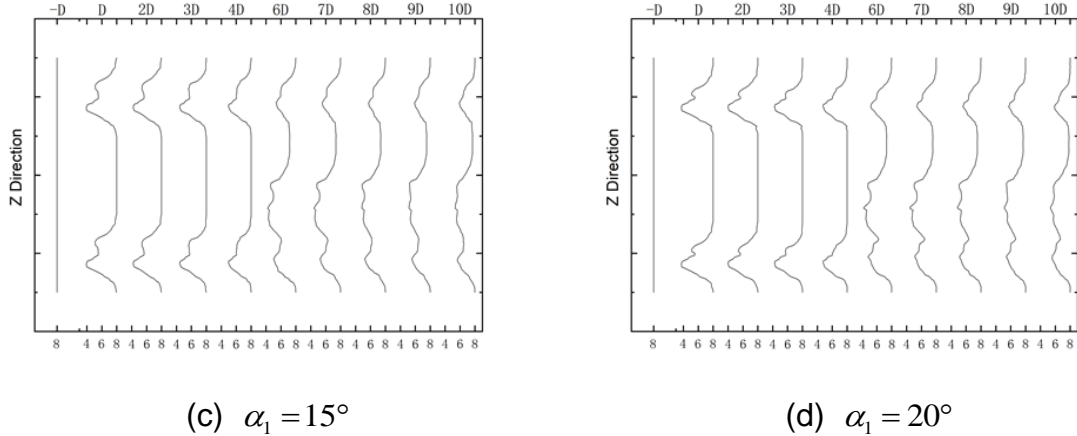


Fig. 8 The Speed Profile in Yaw

It can be seen from the first four curves that the speed difference of two sides of blade rises obviously as the yaw angle increasing, the maximum of which is about $1.6m/s$. The area behind the front two wind turbines is more affected by the first one in the first row. Therefore, the region of the rear wind turbine in the wakes of the first one in the first row is larger increasingly as increase of the yaw angle. The flow field become more complex in the area closed to the first one combined with effect of the rear one, while the other region is stable relatively. Besides, the wind speed in the far field in the different yaw angles are similar.

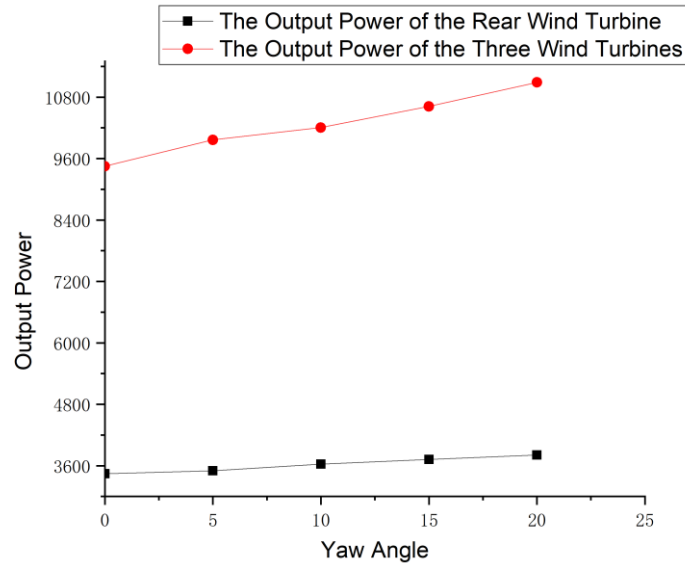


Fig. 9 Total Output Power

As the yaw angle increasing, the output power of the downstream wind turbine increases continuously. Especially when the yaw angle reaches to 20° , the output power is up to the maximum. In the period of the yaw angle increases, the downstream one gradually changes from the state that the two upstream wind turbines commonly affect it to the state that the first one influences its incoming flow mainly by the wake of

the first one. On the one hand, yaw angle can change the flow direction of wind turbines and affect the whole flow field distribution. On the other hand, it increases the distance where the wake of the upstream one affects the downstream one, and reduces the turbulence intensity caused by wake interference. Therefore, the output power of the downstream one is improved relatively.

Theoretically, when yaw angle exceeds a limit value, it is almost completely in the wake area of the first upstream one. And its output power may reduce relatively, but the results is not presented like that. One of the possible reasons is that the yaw angle studied may be not wide enough. And the second one is that the influence of the distance between the first front one and the rear one may be much more than that of whether it is totally behind the wakes area of the first front one. When there is no yaw and the stagger distance is zero, the downstream one is located directly behind the wake area of the first one as well. However, when yaw angle reaches to 20° , the output power is even lower due to its higher turbulence intensity, compared with the former.

5. CONCLUSIONS

In the case of maintaining the fixed space between the different rows and ranks in the wind farm, the flow characteristics and facilities performance of the three wind turbines with inverted-triangle distribution are researched by adopting ALM. The optimum stagger distance without yaw is obtained by changing the relative distance between the downstream wind turbine and the first wind turbine in the upstream. Based on it, the influence of wakes superposition of the two upstream wind turbines in the case of yaw is considered.

The numerical simulation illustrated that the wakes interference effect of the two upstream wind turbines is extremely remarkable. In the case of no yaw, the rear wind turbine is gradually situated from the wakes zone of the first one in the front row to the wake interference zone of the two wind turbines as the stagger distance between the first wind turbine in the first row and downstream one increasing. The growth rate of the output power is improved relatively to the previous process. However, the improvement is limited due to the wake interference effect. Especially when the stagger distance reaches at $4D/3$, the power growth and total power are up to the maximum.

As the yaw angle increasing, the output power of the downstream wind turbine increases continuously, and the output power is up to the maximum, when the yaw angle reaches to 20° . In the period of the yaw angle increases, the downstream one gradually changes from the state that the two upstream wind turbines commonly affect it to the state that the first one influences its incoming flow mainly by the wake of the first one.

According to the wind speed profile above, the interference scope of two wind turbines in the same row could be determined in the case of no yaw. Meanwhile, the optimum stagger distance without yaw can be obtain. Also, the situations of different angles could be analyzed. It could provide a reference value to spatial layout of the complete wind farm.

REFERENCES

1. Leung, D.Y.C. and Y. Yang (2012). *Wind energy development and its environmental impact: A review*. Renewable & Sustainable Energy Reviews. **16**(1): p. 1031-1039.
2. Vermeer, L.J., J.N. Sørensen, and A. Crespo (2003). *Wind turbine wake aerodynamics*. Progress in Aerospace Sciences. **39**(6): p. 467-510.
3. Sanderse, B., S.P. Pijl, and B. Koren (2011). *Review of computational fluid dynamics for wind turbine wake aerodynamics*. Wind Energy. **14**(7): p. 799-819.
4. Lee, S., et al. (2011). *Atmospheric and Wake Turbulence Impacts on Wind Turbine Fatigue Loadings*. Boundary Layers. **135**(3): p. 14-16.
5. Kim, S.H., et al. (2015). *A study of the wake effects on the wind characteristics and fatigue loads for the turbines in a wind farm*. Renewable Energy. **74**: p. 536-543.
6. Shenkar, R. (2010). *Design and Optimization of Planar and Nonplanar Wind Turbine Blades Using Vortex Methods Master Thesis*.
7. Jimenez, A., et al. (2007). *Advances in large-eddy simulation of a wind turbine wake*.
8. Jiménez, Á., A. Crespo, and E. Migoya (2010). *Application of a LES technique to characterize the wake deflection of a wind turbine in yaw*. Wind Energy. **13**(6): p. 559-572.
9. KROGSTAD, et al. (2013). *Blind test calculations of the performance and wake development for a model wind turbine*. Renewable Energy. **50**: p. 325-333.
10. PIERELLA, et al. (2014). *Blind Test 2 calculations for two in-line model wind turbines where the downstream turbine operates at various rotational speeds*. Renewable Energy. **70**(5): p. 62-77.
11. Krogstad, P.Å., L. Sætran, and M.S. Adaramola (2015). *“Blind Test 3” calculations of the performance and wake development behind two in-line and offset model wind turbines*. Journal of Fluids & Structures. **52**(1): p. 65-80.
12. Fleming, P., et al. (2015). *Simulation comparison of wake mitigation control strategies for a two-turbine case*. Wind Energy, 2015. **18**(12): p. 2135-2143.
13. Draper, M., et al. (2018). *A Large Eddy Simulation-Actuator Line Model framework to simulate a scaled wind energy facility and its application*. Journal of Wind Engineering and Industrial Aerodynamics. **182**: p. 146-159.
14. SoRensen, J.N.R. and W.Z. Shen (2002). *Numerical Modeling of Wind Turbine Wakes*. Journal of Fluids Engineering. **124**(2): p. 393.
15. JangOh, CHOUDHRY, Amanullah, et al. (2013). *Large eddy simulation of the wind turbine wake characteristics in the numerical wind tunnel model[J]*. Journal of Wind Engineering & Industrial Aerodynamics. **112**(112):11-24.
16. Wang Shengjun. (2014). *Research on Wake Characteristics of Wind Turbine Based on Actuator Line Model [D]*. Graduate School of Chinese Academy of Sciences (Institute of Engineering Thermophysics).
17. Ai Yong, Cheng Ping, Wan Decheng. (2018). *Numerical Simulation of Wake Field of Two Stagger Wind Turbines Based on Actuator Line Model [J]*. Ocean engineering. **36**(01):27-36